Decay of vector-vector resonances into γ and a pseudoscalar meson

R. Molina,[1] H. Nagahiro,[2] A. Hosaka,[3] and E. Oset[1]

[1]*Departamento de Física Teórica and IFIC, Centro Mixto Universidad de Valencia-CSIC, Institutos de Investigación de Paterna, Apartado 22085, 46071 Valencia, Spain*

[2]*Department of Physics, Nara Women's University, Nara 630-8506, Japan*

[3]*Research Center for Nuclear Physics (RCNP), Osaka University, Ibaraki, Osaka 567-0047, Japan*

(Received 24 September 2010; revised manuscript received 17 March 2011; published 26 May 2011)

We study the decay of dynamically generated resonances from the interaction of two vectors into a γ and a pseudoscalar meson. The dynamics requires anomalous terms involving vertices with two vectors and a pseudoscalar, which renders it special. We compare our result with data on $K_2^{*+}(1430) \to K^+\gamma$ and $K_2^{*0}(1430) \to K^0\gamma$ and find a good agreement with the data for the $K_2^{*+}(1430)$ case and a width considerably smaller than the upper bound measured for the $K_2^{*0}(1430)$ meson. We also investigate the decay into $\pi^+\gamma$ of one a_2 state, tentatively associated to the $a_2(1320)$, obtaining qualitative agreement with data.

DOI: 10.1103/PhysRevD.83.094030 PACS numbers: 13.20.Eb, 13.20.Jf, 13.75.Lb, 14.40.Rt

I. INTRODUCTION

The radiative decay of a mesonic state has long been argued to be crucial in the determination of the nature of the state [1]. For instance, the nonobservation of the $f_0(1500)$ decaying into two photons has been used to support its dominant glue nature [2]. In this sense the radiative decay has also been advocated as a tool to determine the molecular nature of many mesonic and baryonic states [3–9].

The dynamical generation of many mesonic states using chiral unitary dynamics [10,11] has stimulated further studies of these decay modes of mesonic states. Though scalar mesons have been for long in the list of dynamically generated mesons from the interaction of two pseudoscalar mesons [12–16], it has been only very recently that the systems of two vector mesons have been investigated [17–21], and many dynamically generated states have appeared which have been associated with known resonances of the PDG [22]. In this sense the $f_0(1370)$, $f_2(1270)$, $f_2'(1525)$, $f_0(1710)$ and $K_2^*(1430)$ were generated in [17,18] from the interaction of the nonet of vector mesons with itself. Similarly, some D^* mesons are generated in [19], the $D_{s2}^*(2573)$ among other states is generated in [21] and some hidden charm states, some of which could be identified with the new X, Y, Z resonances recently reported, were also found in [20]. The task of studying several radiative decay modes is important for these states in view of the fact that many of them have traditionally been accommodated within quark models without much difficulty [23–29]. Support for the new nature of these states comes gradually from studies of different decay modes. In this sense in [30] the radiative decay of the $f_0(1370)$ and $f_2(1270)$ resonances into $\gamma\gamma$, was studied and good results compared with experiment were found. These studies were extended to the SU(3) states, and also good agreement with experiment was found in the cases where there was available data for comparison [31]. The study of the $J/\psi \to \phi(\omega)f_2(1270)$, $J/\psi \to \phi(\omega)f_2'(1525)$ and $J/\psi \to K^{*0}(892)\bar{K}_2^{*0}(1430)$ decay in [32], and J/ψ decay into $\gamma f_2(1270)$, $\gamma f_2'(1525)$, $\gamma f_0(1370)$ and $\gamma f_0(1710)$ in [33] has given extra support to the claimed nature of these resonances as vector-vector bound states or resonances.

In this paper we pose a new challenge to this idea by investigating the decay of the dynamically generated states of [18] into a pseudoscalar meson and one photon. As we shall see, the decay proceeds via anomalous interaction terms which involve two vectors and a pseudoscalar meson, and thus one is exploring dynamics quite different from the one needed in other alternative studies, like in quark models.

Although there are not many data to compare, we shall see that the agreement with them is satisfactory, within theoretical and experimental uncertainties, and the results obtained should encourage further theoretical and experimental studies in other sectors, like charm or hidden charm mesons.

II. FORMALISM

In this work we study the radiative decay of the VV dynamically generated resonances found in [18] into $P\gamma$. In Table I, we display the masses and widths obtained in that work and the experimental counterpart of each resonance in the assignment made in [18]. We see in this table that 11 resonances were found, five of them were associated with resonances that appear in the PDG [22]. First of all, we consider all the possible cases of spin-parity of the initial meson in Table I: In case we had an initial meson with $J^P = 0^+$, the angular momentum between the pseudoscalar meson and photon should be $L = 1$, which implies negative parity in the final state, and is not allowed. In the language of photon multipoles this corresponds to an M0 transition, which does not exist. The rest of the resonances in Table I are either with or without strangeness.

TABLE I. The properties, (mass, width) [in units of MeV], of the 11 dynamically generated states and, if existing, of those of their PDG counterparts. Theoretical masses and widths are obtained from two different ways: ''pole position'' denotes the numbers obtained from the pole position on the complex plane, where the mass corresponds to the real part of the pole position and the width corresponds to twice the imaginary part of the pole position (the box diagrams corresponding to decays into two pseudoscalars are not included); ''real axis'' denotes the results obtained from the real axis amplitudes squared, where the mass corresponds to the energy at which the amplitude squared has a maximum and the width corresponds to the difference between the two energies, where the amplitude squared is half of the maximum value.

$I^G(J^{PC})$	Theory Pole position	Real axis $\Lambda_b = 1.4$ GeV	Real axis $\Lambda_b = 1.5$ GeV	PDG data Name	Mass	Width
$0^+(0^{++})$	(1512,51)	(1523 257)	(1517 396)	$f_0(1370)$	1200–1500	200–500
$0^+(0^{++})$	(1726,28)	(1721 133)	(1717 151)	$f_0(1710)$	1724 ± 7	137 ± 8
$0^-(1^{+-})$	(1802,78)	(1802,49)		h_1		
$0^+(2^{++})$	(1275,2)	(1276,97)	(1275 111)	$f_2(1270)$	1275.1 ± 1.2	$185.0^{+2.9}_{-2.4}$
$0^+(2^{++})$	(1525,6)	(1525,45)	(1525,51)	$f_2'(1525)$	1525 ± 5	73^{+6}_{-5}
$1^-(0^{++})$	(1780 133)	(1777 148)	(1777 172)	a_0		
$1^+(1^{+-})$	(1679 235)	(1703 188)		b_1		
$1^-(2^{++})$	(1569,32)	(1567,47)	(1566,51)	$a_2(1320)$?		
$1/2(0^+)$	(1643,47)	(1639 139)	(1637 162)	K_0^*		
$1/2(1^+)$	(1737 165)	(1743 126)		$K_1(1650)$?		
$1/2(2^+)$	(1431,1)	(1431,56)	(1431,63)	$K_2^*(1430)$	1429 ± 1.4	104 ± 4

The ones without strangeness except for those of $J = 1$ have positive C-parity which does not allow the decay into $P\gamma$. This leaves nonvanishing decay rates only for the h_1, b_1, K_1 and $K_2^*(1430)$, with only the latter one having a clear experimental counterpart, the $K_2^*(1430)$. In the present work we concentrate on this case, where there are also experimental data in the PDG for its decay into $P\gamma$:

$$\Gamma(K_2^{*+}(1430) \to K^+\gamma)/\Gamma = (2.4 \pm 0.5) \times 10^{-3}$$
$$\Gamma(K_2^{*0}(1430) \to K^0\gamma)/\Gamma < 9 \times 10^{-4}. \quad (1)$$

In [18] there was also one a_2 resonance found at around 1560 MeV, which was compared with the $a_2(1700)$ for the proximity of the masses, but serious problems with the widths were observed. Here we shall assume that the $a_2(1560)$ found in [18] corresponds to the experimental $a_2(1320)$ and we will also evaluate the radiative width into $\pi^+\gamma$. Experimentally we have

$$\Gamma(a_2(1320) \to \pi^+\gamma)/\Gamma = (2.68 \pm 0.31) \times 10^{-3}. \quad (2)$$

The difference of the masses between the $a_2(1560)$ found and the experimental $a_2(1320)$ could be reduced in [18] with some fine-tuning of the subtraction constants, but we shall not do it here.

From [18] we take the channels and coupling constants, g_i, of the $K_2^*(1430)$ and $a_2(1320)$ ($a_2(1569)$ in [18]), that are shown in Table II. As we see in this table, the $K_2^*(1430)$ couples to three channels: ρK^*, $K^*\omega$ and $K^*\phi$, the coupling to ρK^* being considerably larger than for the other two channels. The $a_2(1320)$ couples to $K^*\bar{K}^*$, $\rho\omega$ and $\rho\phi$, the largest coupling corresponding to $K^*\bar{K}^*$.

In Fig. 1 we show the two kinds of Feynman diagrams that lead to the decay of a resonance into $P\gamma$ in the VV molecular picture that combines HGS (hidden local gauge symmetry) [34–38] and unitarity [17,18]. The two different diagrams contain an anomalous VVP coupling, whereas they can be distinguished from the exchange of one pseudoscalar meson, P_l, containing a PPV vertex, see Fig. 1(a), or a vector meson, V_l, with a $3V$ vertex, as shown in Fig. 1(b). These two kinds of diagrams lead to four possible configurations, as shown in Fig. 2 for the ρK^* channel, depending on whether $P_l(V_l)$ is a nonstrange meson, Fig. 2(a) and 2(b), or a strange meson, Fig. 2(c) and 2(d). At the end, all possible VV channels are taken into account. In this case, only a few diagrams contribute so we show all the possibilities.

For the case of the $a_2(1320)$ the corresponding diagrams are shown in Fig. 3.

The $V\gamma$, PPV and $3V$ vertices are provided by the hidden gauge formalism, where a photon always comes out from a vector meson. In the HGS formalism, the vector meson fields are gauge bosons of a hidden local symmetry transforming inhomogeneously and chiral symmetry is preserved [34–38]. The HGS Lagrangian involving pseudoscalar, vector mesons and photons is

TABLE II. Pole positions and residues in the strangeness = 0 and isospin = 0 channel. All the quantities are in units of MeV.

$\sqrt{s}_{\text{pole}}$	g_i [spin = 2]		
	$K^*\rho$	$K^*\omega$	$K^*\phi$
$(1431, -i1)$	$(10901, -i71)$	$(2267, -i13)$	$(-2898, i17)$
	$K^*\bar{K}^*$	$\rho\omega$	$\rho\phi$
$(1569, -i16)$	$(10208, -i337)$	$(-4598, i451)$	$(6052, -i604)$

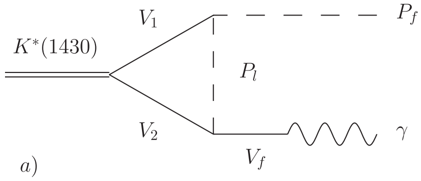

FIG. 1. The two different diagrams that contribute to the $K_2^*(1430) \to K\gamma$ decay.

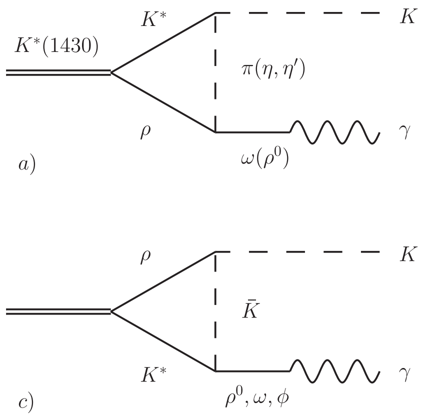

FIG. 2. Possible Feynman diagrams contributing to the $K_2^*(1430) \to K\gamma$ decay in the ρK^* channel.

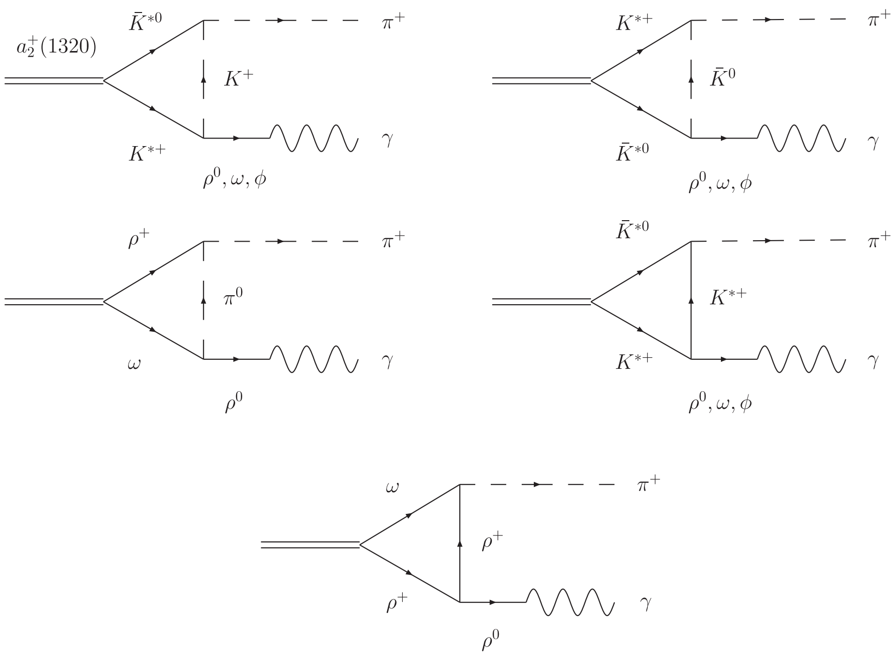

FIG. 3. Possible Feynman diagrams contributing to the $a_2^{*+}(1320) \to \pi^+\gamma$ decay.

$$\mathcal{L} = \mathcal{L}^{(2)} + \mathcal{L}_{III} \tag{3}$$

with

$$\mathcal{L}^{(2)} = \frac{1}{4} f^2 \langle D_\mu U D^\mu U^\dagger + \chi U^\dagger + \chi^\dagger U \rangle \tag{4}$$

$$\mathcal{L}_{III} = -\frac{1}{4}\langle V_{\mu\nu} V^{\mu\nu}\rangle + \frac{1}{2} M_V^2 \left\langle \left[V_\mu - \frac{i}{g}\Gamma_\mu \right]^2 \right\rangle, \tag{5}$$

where $\langle \ldots \rangle$ represents a trace over SU(3) matrices. The covariant derivative is defined by

$$D_\mu U = \partial_\mu U - ieQA_\mu U + ieUQA_\mu, \quad (6)$$

with $Q = \mathrm{diag}(2, -1, -1)/3$, $e = -|e|$ the electron charge, and A_μ the photon field. The chiral matrix U is given by

$$U = e^{i\sqrt{2}P/f}, \quad (7)$$

where the P matrix contains the nonet of the pseudoscalars in the physical basis considering η, η' mixing [39]:

$$P = \begin{pmatrix} \frac{\eta}{\sqrt{3}} + \frac{\eta'}{\sqrt{6}} + \frac{\pi^0}{\sqrt{2}} & \pi^+ & K^+ \\ \pi^- & \frac{\eta}{\sqrt{3}} + \frac{\eta'}{\sqrt{6}} - \frac{\pi^0}{\sqrt{2}} & K^0 \\ K^- & \bar{K}^0 & -\frac{\eta}{\sqrt{3}} + \sqrt{\frac{2}{3}}\eta' \end{pmatrix}, \quad (8)$$

and V_μ represents the vector nonet:

$$V_\mu = \begin{pmatrix} \frac{\omega+\rho^0}{\sqrt{2}} & \rho^+ & K^{*+} \\ \rho^- & \frac{\omega-\rho^0}{\sqrt{2}} & K^{*0} \\ K^{*-} & \bar{K}^{*0} & \phi \end{pmatrix}_\mu. \quad (9)$$

In $\mathcal{L}_{III}$, $V_{\mu\nu}$ is defined as

$$V_{\mu\nu} = \partial_\mu V_\nu - \partial_\nu V_\mu - ig[V_\mu, V_\nu] \quad (10)$$

and

$$\Gamma_\mu = \frac{1}{2}[u^\dagger(\partial_\mu - ieQA_\mu)u + u(\partial_\mu - ieQA_\mu)u^\dagger] \quad (11)$$

with $u^2 = U$. The value of the coupling constant g of the Lagrangian Eq. (5) satisfies

$$g = \frac{M_V}{2f}, \quad (12)$$

with M_V the vector meson mass and $f = 93$ MeV the pion decay constant. Other properties of g are [38,40]:

$$\frac{F_V}{M_V} = \frac{1}{\sqrt{2}g}, \qquad \frac{G_V}{M_V} = \frac{1}{2\sqrt{2}g},$$
$$F_V = \sqrt{2}f, \qquad G_V = \frac{f}{\sqrt{2}}. \quad (13)$$

Equation (5) provides the following terms:

$$\mathcal{L}_{V\gamma} = -M_V^2 \frac{e}{g} A_\mu \langle V^\mu Q\rangle$$
$$\mathcal{L}_{PPV} = -ig\langle V^\mu [P, \partial_\mu P]\rangle \quad (14)$$

and

$$\mathcal{L}_{3V} == ig\langle (V^\mu \partial_\nu V_\mu - \partial_\nu V_\mu V^\mu) V^\nu)\rangle. \quad (15)$$

Both diagrams in Fig. 1 contain an anomalous VVP vertex, which in principle one could expect to be small due to the higher order nature of the anomalous term in the chiral expansion. This anomalous VVP interaction accounts for a process that does not preserve intrinsic parity, and can be obtained from the gauged Wess-Zumino term (see e.g. [41,42]). However, as the relevant energy becomes larger, the role of the anomalous contribution becomes more important as it contains momentum factors (see Eq. (16)). This has also been seen in works on the radiative decays of scalar mesons [43,44]. The VVP Lagrangian is [42,45,46]:

$$\mathcal{L}_{VVP} = \frac{G'}{\sqrt{2}} \epsilon^{\mu\nu\alpha\beta} \langle \partial_\mu V_\nu \partial_\alpha V_\beta P\rangle \quad (16)$$

with $G' = 3g'^2/(4\pi^2 f)$ and $g' = -G_V M_\rho/(\sqrt{2}f^2)$. In the following subsections we evaluate the two different kinds of diagrams shown in Fig. 1.

A. Diagram of the $K^*(1430) \to K\gamma$ decay containing the PPV vertex

In Fig. 4 we show the first diagram to compute in charge basis with explicit momentum. In what follows, we shall consider the $K_2^{*+}(1430)$ at rest. First of all, we need the coupling of the resonance $K_2^{*+}(1430)$ to $K^{*0}\rho^+$. This coupling is given by the approach of [18], where the coupling is calculated as the residue of the $VV \to VV$ amplitude in the pole position of the resonance (see Fig. 5), which close to a pole can be expressed as:

$$t_{rs}^{(J=2)ij} = \frac{g_r g_s}{s - s_{\mathrm{pole}}} \left\{\frac{1}{2}(\epsilon^{(1)i}\epsilon^{(2)j} + \epsilon^{(1)j}\epsilon^{(2)i}) - \frac{1}{3}\epsilon^{(1)l}\epsilon^{(2)l}\delta^{ij}\right\} \times \left\{\frac{1}{2}(\epsilon^{(1)i}\epsilon^{(2)j} + \epsilon^{(1)j}\epsilon^{(2)i}) - \frac{1}{3}\epsilon^{(1)m}\epsilon^{(2)m}\delta^{ij}\right\}, \quad (17)$$

with $s_{\mathrm{pole}} = (M - i\Gamma/2)^2$. We can see in this amplitude, by looking at the diagram in Fig. 5, that the coupling

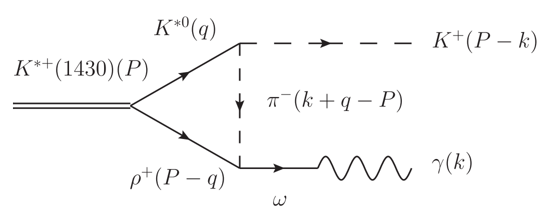

FIG. 4. Feynman diagram of the $K_2^{*+}(1430) \to K^+\gamma$ decay in the $\rho^+ K^{*0}$ channel with a PPV vertex.

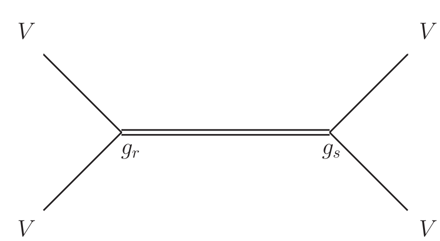

FIG. 5. Dynamically generated resonance from the VV interaction

of the resonance to a VV channel is given by $\tilde{g}_r = g_r\{\frac{1}{2}(\epsilon^{(1)i}\epsilon^{(2)j} + \epsilon^{(1)j}\epsilon^{(2)i}) - \frac{1}{3}\epsilon^{(1)l}\epsilon^{(2)l}\delta^{ij}\}$, r or s corresponding to one of the channels ρK^*, ωK^* or ϕK^*. These couplings are given in Table II in the isospin basis and we have to multiply them for the correspondent Clebsch Gordan coefficient:

$$|\rho K^*, 1/2, 1/2\rangle = -\sqrt{\frac{2}{3}}\rho^+ K^{*0} - \frac{1}{\sqrt{3}}\rho^0 K^{*+}$$
$$|\rho K^*, 1/2, -1/2\rangle = -\sqrt{\frac{2}{3}}\rho^- K^{*+} + \frac{1}{\sqrt{3}}\rho^0 K^{*0}. \tag{18}$$

The isospin coefficient is denoted as g_I. Thus, from Eqs. (14)–(17) we can write the vertices involved in the diagram of Fig. 4 as

$$t^{ij}_{RV_1V_2} = g_I g_r\left\{\frac{1}{2}(\epsilon^{(1)i}\epsilon^{(2)j} + \epsilon^{(1)j}\epsilon^{(2)i}) - \frac{1}{3}\epsilon^{(1)l}\epsilon^{(2)l}\delta^{ij}\right\}$$
$$t_{V_f\gamma} = \lambda\frac{e}{g}M^2_{V_f}\epsilon^{(\gamma)}_\mu\epsilon^{(f)\mu}$$
$$t_{P_lP_fV_1} = Ag(p_{\rm in} + p_{\rm fin})_\mu\epsilon^{(1)\mu} = -Ag(2(P-k)-q)_\mu\epsilon^{(1)\mu}$$
$$t_{V_2V_fP_l} = -B\frac{G'}{\sqrt{2}}\epsilon^{\alpha\beta\gamma\delta}(P-q)_\alpha\epsilon^{(2)}_\beta k_\gamma\epsilon^{(f)}_\delta, \tag{19}$$

with $V_1 = K^{*0}$, $V_2 = \rho^+$, $V_f = \omega$, $P_l = \pi^-$, $P_f = K^+$, and the coefficients g_I, g_r, A, B and λ are $-\sqrt{\frac{2}{3}}$, $(10901, -i71)$ MeV, -1, $\sqrt{2}$ and $\frac{1}{3\sqrt{2}}$ respectively. The $V_f \to \gamma$ conversion essentially replaces, up to a constant, $\epsilon^{(f)}_\delta$ by $\epsilon^{(\gamma)}_\delta$. Therefore, we can write the amplitude of the diagram depicted in Fig. 4 as

$$-it^{ij}_{K_2^{*+}(1430)\to K^+\gamma} = \int\frac{d^4q}{(2\pi)^4}\left\{\frac{1}{2}(\epsilon^{(1)i}\epsilon^{(2)j} + \epsilon^{(1)j}\epsilon^{(2)i}) - \frac{1}{3}\epsilon^{(1)}_l\epsilon^{(2)}_l\delta^{ij}\right\}\epsilon^{(1)\mu}(2(P-k)-q)_\mu\epsilon^{\alpha\beta\gamma\delta}(P-q)_\alpha\epsilon^{(2)}_\beta k_\gamma\epsilon^{(\gamma)}_\delta$$
$$\times\frac{1}{q^2 - M_1^2 + i\epsilon}\frac{1}{(k+q-P)^2 - m_l^2 + i\epsilon}\frac{1}{(P-q)^2 - M_2^2 + i\epsilon}\times F_I\times eg_rG', \tag{20}$$

with $M_1 = m_{K^*}$, $M_2 = m_\rho$, $m_l = m_\pi$ and $\mathrm{F_I} = \frac{1}{\sqrt{2}}AB\lambda g_I = \frac{1}{3\sqrt{3}}$. We should be consistent with the approximation done in [17,18], where $|\vec{q}|/M_1 \simeq 0$, which implies that $\epsilon^{(1)0} \simeq 0$. This means that the μ and β indices should be spatial and also that the q^iq^j/M_V^2 terms in the sum over vector polarizations should be neglected. For convenience, we will keep them as covariant indices and will consider them as spatial indices at the end. Thus, after summing over polarizations

$$\sum_\lambda\epsilon^{(1)i}\epsilon^{(1)\mu} = -g^{i\mu} \qquad \sum_\lambda\epsilon^{(2)j}\epsilon^{(2)}_\beta = -g^j_\beta, \tag{21}$$

we get

$$-it^{ij}_{K_2^{*+}(1430)\to K^+\gamma} = \int\frac{d^4q}{(2\pi)^4}\left\{\frac{1}{2}\epsilon^{\alpha j\gamma\delta}(2(P-k)-q)^i(P-q)_\alpha k_\gamma\epsilon^{(\gamma)}_\delta + \frac{1}{2}\epsilon^{\alpha i\gamma\delta}(2(P-k)-q)^j(P-q)_\alpha k_\gamma\epsilon^{(\gamma)}_\delta\right.$$
$$\left.-\frac{1}{3}\epsilon^{\alpha m\gamma\delta}(2(P-k)-q)^m(P-q)_\alpha k_\gamma\epsilon^{(\gamma)}_\delta\delta^{ij}\right\}\frac{1}{q^2 - M_1^2 + i\epsilon}\frac{1}{(k+q-P)^2 - m_l^2 + i\epsilon}$$
$$\times\frac{1}{(P-q)^2 - M_2^2 + i\epsilon}\times\mathrm{F_I}\times eg_rG'. \tag{22}$$

All the terms of Eq. (22) are proportional to an integral like

$$\int\frac{d^4q}{(2\pi)^4}(2(P-k)-q)^i(P-q)_\alpha\frac{1}{q^2 - M_1^2 + i\epsilon}\frac{1}{(k+q-P)^2 - m_l^2 + i\epsilon}\frac{1}{(P-q)^2 - M_2^2 + i\epsilon}, \tag{23}$$

which from Lorentz covariance must be a tensor built from P and k,

$$ag^i_\alpha + bP^iP_\alpha + ck^iP_\alpha + dP^ik_\alpha + ek^ik_\alpha. \tag{24}$$

The second and fourth terms in Eq. (24) vanish directly because $P^i = 0$. After substituting the integrals of Eq. (22) by Eq. (24) with the correspondent indices, we see that the first term in Eq. (24) leads to a term proportional to

$$\frac{1}{2}k_\gamma\epsilon^{(\gamma)}_\delta a(\epsilon^{ij\gamma\delta} + \epsilon^{ji\gamma\delta}) - \frac{1}{3}\epsilon^{\alpha m\gamma\delta}k_\gamma\epsilon^{(\gamma)}_\delta\delta^{ij}ag^m{}_\alpha. \tag{25}$$

This term vanishes when one contracts the antisymmetric operator $\epsilon^{\alpha m\gamma\delta}$ with the symmetric g^m_α. This is a welcome feature because this term of the integral in Eq. (23) was the only one that is divergent. The fifth term, ek^ik_α, leads to terms proportional to $k_\gamma k_\alpha\epsilon^{\alpha l\gamma\delta}$, and therefore it also vanishes. The third term, ck^iP_α, is the only one that remains, but we can still simplify it a little bit. The integral in Eq. (22) is proportional to

$$\frac{1}{2}cP_\alpha k_\gamma \epsilon_\delta^{(\gamma)}(k^i\epsilon^{\alpha j\gamma\delta}+k^j\epsilon^{\alpha i\gamma\delta})-\frac{1}{3}c\epsilon^{\alpha m\gamma\delta}k_\gamma\delta^{ij}\epsilon_\delta^{(\gamma)}k^mP_\alpha. \tag{26}$$

The last term in the above equation vanishes for $P^i=0$. To see it, let us split the factor $\epsilon^{\alpha m\gamma\delta}k_\gamma k^m P_\alpha$ in two terms

$$\sum_{m=1,3}\epsilon^{\alpha m0\delta}k_0k^mP_\alpha+\sum_{m=1,3}\sum_{l=1,3}\epsilon^{\alpha ml\delta}k_lk^mP_\alpha; \tag{27}$$

the last term is zero since it is a product of an antisymmetric operator with a symmetric one. In addition, the presence of P_α forces $\alpha=0$, which makes the first term also disappear.

Now we must evaluate the c coefficient. Let us use the formula of the Feynman parametrization for $n=3$

$$\frac{1}{\alpha\beta\gamma}=2\int_0^1dx\int_0^xdy\frac{1}{[\alpha+(\beta-\alpha)x+(\gamma-\beta)y]^3}. \tag{28}$$

For the integral of Eq. (23), we can use the above parametrization with

$$\begin{aligned}\alpha&=q^2-M_1^2\\ \beta&=(P-q)^2-M_2^2\\ \gamma&=(P-q-k)^2-m_l^2.\end{aligned} \tag{29}$$

Besides this, we define a new variable $q'=q-Px+ky$, such that the integral of Eq. (23) can be expressed as

$$2\int\frac{d^4q'}{(2\pi)^4}\int_0^1dx\int_0^xdy(2(P-k)-q)^i(P-q)_\alpha\frac{1}{(q'^2+s)^3}, \tag{30}$$

with

$$\begin{aligned}s={}&-(P^0)^2x^2+2P^0k^0xy+((P^0)^2-M_2^2+M_1^2)x\\&+(-2P^0k^0+M_2^2-m_l^2)y-M_1^2.\end{aligned} \tag{31}$$

From Eq. (30), we must take the k^iP_α term. Therefore,

$$c=2\int\frac{d^4q'}{(2\pi)^4}\int_0^1dx\int_0^xdy\frac{(1-x)(y-2)}{(q'^2+s)^3}. \tag{32}$$

Now we still can perform the integral in the q' variable analytically:

$$\int d^4q'\frac{1}{(q'^2+s)^3}=\frac{i\pi^2}{2s}, \tag{33}$$

and finally, we get

$$c=\frac{i}{16\pi^2}\int_0^1dx\int_0^xdy\frac{(1-x)(y-2)}{s}, \tag{34}$$

and the amplitude of the diagram of Fig. 4 as

$$\begin{aligned}&-it^{ij}_{K_2^{*+}(1430)\to K^+\gamma}\\&\quad=\frac{1}{2}cP_\alpha k_\gamma\epsilon_\delta^{(\gamma)}(k^i\epsilon^{\alpha j\gamma\delta}+k^j\epsilon^{\alpha i\gamma\delta})\mathrm{F_I}eg_rG'.\end{aligned} \tag{35}$$

B. Diagram of the $K^*(1430)\to K\gamma$ decay containing the $3V$ vertex

Now, we want to compute the second diagram for the $K^*(1430)\to K\gamma$ decay depicted in Fig. 2. In Fig. 6 we show this diagram with the explicit momenta in the case of the $K^{*0}\rho^+$ intermediate state. The difference with the diagram calculated in the previous section is the presence of the $3V$ vertex, which we can obtain from the Lagrangian of Eq. (15). This vertex and the anomalous VVP vertex are

$$\begin{aligned}t_{V_2V_lV_f}={}&gD\{(2k+q-P)_\mu\epsilon_\nu^{(l)}\epsilon^{(2)\mu}\epsilon^{(f)\nu}\\&-(k+P-q)_\mu\epsilon_\nu^{(2)}\epsilon^{(l)\mu}\epsilon^{(f)\nu}\\&+(2(P-q)-k)_\mu\epsilon_\nu^{(l)}\epsilon^{(f)\mu}\epsilon^{(2)\nu}\}\\ t_{V_1V_lP_f}={}&-B\frac{G'}{\sqrt{2}}\epsilon^{\alpha\beta\gamma\delta}q_\alpha\epsilon_\beta^{(1)}(k+q-P)_\gamma\epsilon_\delta^{(l)},\end{aligned} \tag{36}$$

with $D=\sqrt{2}$, $B=1$, and g_I, g_r, λ in Eqs. (19) are $-\sqrt{\frac{2}{3}}$, $(10901,-i71)$ MeV, $\frac{1}{\sqrt{2}}$ respectively. With this, we can write the amplitude of the diagram in Fig. 6 as

$$\begin{aligned}-it^{ij}_{K_2^{*+}(1430)\to K^+\gamma}={}&\int\frac{d^4q}{(2\pi)^4}\left\{\frac{1}{2}(\epsilon^{(1)i}\epsilon^{(2)j}+\epsilon^{(1)j}\epsilon^{(2)i})-\frac{1}{3}\epsilon_l^{(1)}\epsilon_l^{(2)}\delta^{ij}\right\}\epsilon^{\alpha\beta\gamma\delta}q_\alpha\epsilon_\beta^{(1)}(k+q-P)_\gamma\\&\times\epsilon_\delta^{(l)}\{(2k+q-P)_\mu\epsilon_\nu^{(l)}\epsilon^{(2)\mu}\epsilon^{(\gamma)\nu}-(k+P-q)_\mu\epsilon_\nu^{(2)}\epsilon^{(l)\mu}\epsilon^{(\gamma)\nu}+(2(P-q)-k)_\mu\epsilon_\nu^{(l)}\epsilon^{(\gamma)\mu}\epsilon^{(2)\nu}\}\\&\times\frac{1}{q^2-M_1^2+i\epsilon}\frac{1}{(k+q-P)^2-M_l^2+i\epsilon}\frac{1}{(P-q)^2-M_2^2+i\epsilon}\times\mathrm{F}'_\mathrm{I}\times eg_rG'\end{aligned} \tag{37}$$

with $\mathrm{F}'_\mathrm{I}=-\frac{1}{\sqrt{2}}g_IBD\lambda$. The way to proceed is very similar to that of the previous subsection, with the only difference in the use of the Lorentz condition, $k_\mu\epsilon^{(\gamma)\mu}=0$. Now, we get two kinds of integrals. The first one is

$$\int\frac{d^4q}{(2\pi)^4}q_\alpha\frac{1}{q^2-M_1^2+i\epsilon}\frac{1}{(k+q-P)^2-M_l^2+i\epsilon}\frac{1}{(P-q)^2-M_2^2+i\epsilon}, \tag{38}$$

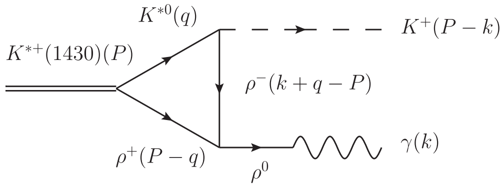

FIG. 6. Feynman diagram of the $K_2^{*+}(1430) \to K^+\gamma$ decay in the $\rho^+ K^{*0}$ channel with a $3V$ vertex.

which from Lorentz covariance takes the form

$$a_1 P_\alpha + b_1 k_\alpha. \tag{39}$$

After contracting with the term $k_\gamma P_\delta \epsilon^{\alpha i \gamma \delta}$, this integral becomes zero. The second integral is

$$\int \frac{d^4 q}{(2\pi)^4} q_\alpha (2k + q - P)^j \frac{1}{q^2 - M_1^2 + i\epsilon} \times \frac{1}{(k+q-P)^2 - M_l^2 + i\epsilon} \frac{1}{(P-q)^2 - M_2^2 + i\epsilon} \tag{40}$$

which takes the form

$$a_2 g_\alpha^j + b_2 k_\alpha k^j + c_2 k^j P_\alpha + d_2 P^j k_\alpha + e_2 P^j P_\alpha. \tag{41}$$

The last two terms are zero since $P^j = 0$, and the first one disappears because it gives rise to the factor $g_\alpha^j \epsilon^{\alpha i \gamma \delta} + g_\alpha^i \epsilon^{\alpha j \gamma \delta} = 0$. The final amplitude is a function of the b_2 and c_2 coefficients, and it can be expressed as

$$-it^{ij}_{K_2^{*+}(1430)\to K^+\gamma} = -\frac{1}{2}(k^j \epsilon^{\alpha i \gamma \delta} + k^i \epsilon^{\alpha j \gamma \delta})\epsilon_\delta^{(\gamma)}(-b_2 k_\alpha P_\gamma + c_2 P_\alpha k_\gamma)\mathrm{F}'_\mathrm{I} e g_r G', \tag{42}$$

with

$$\begin{aligned} b_2 &= \frac{i}{16\pi^2}\int_0^1 dx \int_0^x dy \frac{y(y-2)}{s'} \\ c_2 &= \frac{i}{16\pi^2}\int_0^1 dx \int_0^x dy \frac{x(2-y)}{s'} \end{aligned} \tag{43}$$

and

$$\begin{aligned} s' = &-(P^0)^2 x^2 + 2P^0 k^0 xy + ((P^0)^2 - M_2^2 + M_1^2)x \\ &+ (-2P^0 k^0 + M_2^2 - M_l^2)y - M_1^2. \end{aligned} \tag{44}$$

The sum of the diagrams in Figs. 4 and 6, from Eqs. (35), (34), (42), and (43), gives rise to the following amplitude:

$$\begin{aligned} -it^{ij}_{K_2^{*+}(1430)\to K^+\gamma} = &\frac{1}{2}(b'_2 k_\alpha P_\gamma + (c' - c'_2) P_\alpha k_\gamma) \\ &\times (k^j \epsilon^{\alpha i \gamma \delta} + k^i \epsilon^{\alpha j \gamma \delta})\epsilon_\delta^{(\gamma)} e G', \end{aligned} \tag{45}$$

with

$$b'_2 = g_r \mathrm{F}'_\mathrm{I} \qquad b_2 c' = g_r \mathrm{F}_\mathrm{I} c \qquad c'_2 = g_r \mathrm{F}'_\mathrm{I} c_2. \tag{46}$$

In order to compute the decay width of the process $K_2^{*+}(1430) \to K^+\gamma$, we need to evaluate the squared amplitude summing over polarizations, i.e., $\frac{1}{2J+1}\sum_{\lambda_f}\sum_{\lambda_i} t_{ij}(t^{ij})^*$. The sum over the polarizations of the photon $\sum_{\lambda_f}\epsilon_\delta^{(\gamma)}\epsilon_{\delta'}^{(\gamma)}$ leads to a factor $-g_{\delta\delta'}$. In addition, products of the antisymmetric $\epsilon^{\alpha\beta\gamma\delta}$ operators appear, for what we make use of the rule

$$\epsilon^{\alpha\beta\gamma\delta}\epsilon^{\alpha'\gamma'}_{\beta'\delta} = -\begin{vmatrix} g^{\alpha\alpha'} & g^{\alpha}_{\beta'} & g^{\alpha\gamma'} \\ g^{\beta\alpha'} & g^{\beta}_{\beta'} & g^{\beta\gamma'} \\ g^{\gamma\alpha'} & g^{\gamma}_{\beta'} & g^{\gamma\gamma'} \end{vmatrix}, \tag{47}$$

with β, β' spatial indices. Finally, we find

$$\frac{1}{2J+1}\sum_{\lambda_f}\sum_{\lambda_i}|t|^2 = \frac{1}{2J+1}|\vec{k}|^4 P_0^2 |b'_2 + c'_2 - c'|^2 (eG')^2. \tag{48}$$

The $K_2^{*+}(1430) \to K^+\gamma$ decay width is

$$\Gamma(K_2^{*+}(1430) \to K^+\gamma) = \frac{1}{8\pi}\frac{1}{2J+1}|\vec{k}|^5 |b'_2 + c'_2 - c'|^2 (eG')^2. \tag{49}$$

We must include not only the $K^*\rho$ channel, but all the possible channels listed in Table II: the $K^*\omega$ and $K^*\phi$ channels. The different F_I, F'_I for each channel r are listed in Tables III, IV, V, VI, VII, VIII, IX, and X in the Appendix. Therefore,

$$\begin{aligned} c' &= \frac{1}{16\pi^2}\int_0^1 dx \int_0^x dy (1-x)(y-2)\sum_r \frac{\mathrm{F}_\mathrm{I}(r) g_r}{s(r)} \\ b'_2 &= \frac{1}{16\pi^2}\int_0^1 dx \int_0^x dy y(y-2)\sum_r \frac{\mathrm{F}'_\mathrm{I}(r) g_r}{s'(r)} \\ c'_2 &= \frac{1}{16\pi^2}\int_0^1 dx \int_0^x dy x(2-y)\sum_r \frac{\mathrm{F}'_\mathrm{I}(r) g_r}{s'(r)}. \end{aligned} \tag{50}$$

For completeness, we show s, s', F_I and F'_I again,

$$\begin{aligned} s = &-(P^0)^2 x^2 + 2P^0 k^0 xy + ((P^0)^2 - M_2^2 + M_1^2)x \\ &+ (-2P^0 k^0 + M_2^2 - m_l^2)y - M_1^2 \\ s' = &-(P^0)^2 x^2 + 2P^0 k^0 xy + ((P^0)^2 - M_2^2 + M_1^2)x \\ &+ (-2P^0 k^0 + M_2^2 - M_l^2)y - M_1^2 \\ \mathrm{F}_\mathrm{I} = &\frac{1}{\sqrt{2}} AB\lambda g_I \\ \mathrm{F}'_\mathrm{I} = &-\frac{1}{\sqrt{2}} g_I BD\lambda. \end{aligned} \tag{51}$$

TABLE III. K^{*+} decay diagrams involving the ρK^* channel and the PPV vertex.

V_1	V_2	P_l	V_f	P_f	A	B	λ	g_I	$\mathrm{F_I}$	Γ_i (KeV)
K^{*0}	ρ^+	π^-	ω	K^+	-1	$\sqrt{2}$	$\frac{1}{3\sqrt{2}}$	$-\sqrt{\frac{2}{3}}$	$\frac{1}{3\sqrt{3}}$	6.05
K^{*+}	ρ^0	π^0	ω	K^+	$-\frac{1}{\sqrt{2}}$	$\sqrt{2}$	$\frac{1}{3\sqrt{2}}$	$-\frac{1}{\sqrt{3}}$	$\frac{1}{6\sqrt{3}}$	
ρ^0	K^{*+}	K^-	ρ^0	K^+	$\frac{1}{\sqrt{2}}$	$\frac{1}{\sqrt{2}}$	$\frac{1}{\sqrt{2}}$	$-\frac{1}{\sqrt{3}}$	$-\frac{1}{4\sqrt{3}}$	5.05
			ω			$\frac{1}{\sqrt{2}}$	$\frac{1}{3\sqrt{2}}$		$-\frac{1}{12\sqrt{3}}$	
			ϕ			1	$-\frac{1}{3}$		$\frac{1}{6\sqrt{3}}$	
ρ^+	K^{*0}	$\bar{K}^0$	ρ^0	K^+	1	$-\frac{1}{\sqrt{2}}$	$\frac{1}{\sqrt{2}}$	$-\sqrt{\frac{2}{3}}$	$\frac{1}{2\sqrt{3}}$	
			ω			$\frac{1}{\sqrt{2}}$	$\frac{1}{3\sqrt{2}}$		$-\frac{1}{6\sqrt{3}}$	
			ϕ			1	$-\frac{1}{3}$		$\frac{1}{3\sqrt{3}}$	
K^{*+}	ρ^0	η	ρ^0	K^+	$-\frac{2}{\sqrt{3}}$	$\frac{2}{\sqrt{3}}$	$\frac{1}{\sqrt{2}}$	$-\frac{1}{\sqrt{3}}$	$\frac{2}{3\sqrt{3}}$	6.78
		η'			$\frac{1}{\sqrt{6}}$	$\sqrt{\frac{2}{3}}$	$\frac{1}{\sqrt{2}}$	$-\frac{1}{\sqrt{3}}$	$-\frac{1}{6\sqrt{3}}$	0.24

TABLE IV. K^{*+} decay diagrams involving the ωK^* and ϕK^* channels and the PPV vertex.

V_1	V_2	P_l	V_f	P_f	A	B	λ	g_I	$\mathrm{F_I}$	Γ_i(KeV)
K^{*+}	ω	π^0	ρ^0	K^+	$-\frac{1}{\sqrt{2}}$	$\sqrt{2}$	$\frac{1}{\sqrt{2}}$	1	$-\frac{1}{2}$	0.77
ω	K^{*+}	K^-	ρ^0	K^+	$\frac{1}{\sqrt{2}}$	$\frac{1}{\sqrt{2}}$	$\frac{1}{\sqrt{2}}$	1	$\frac{1}{4}$	0.07
			ω			$\frac{1}{\sqrt{2}}$	$\frac{1}{3\sqrt{2}}$		$\frac{1}{12}$	
			ϕ			1	$-\frac{1}{3}$		$-\frac{1}{6}$	
K^{*+}	ω	η	ω	K^+	$-\frac{2}{\sqrt{3}}$	$\frac{2}{\sqrt{3}}$	$\frac{1}{3\sqrt{2}}$	1	$-\frac{2}{9}$	9.5×10^{-2}
			ϕ						0	
		η'	ω		$\frac{1}{\sqrt{6}}$	$\sqrt{\frac{2}{3}}$	$\frac{1}{3\sqrt{2}}$	1	$\frac{1}{18}$	3.2×10^{-3}
			ϕ						0	
ϕ	K^{*+}	K^-	ρ^0	K^+	-1	$\frac{1}{\sqrt{2}}$	$\frac{1}{\sqrt{2}}$	1	$-\frac{1}{2\sqrt{2}}$	8.4×10^{-2}
			ω			$\frac{1}{\sqrt{2}}$	$\frac{1}{3\sqrt{2}}$		$-\frac{1}{6\sqrt{2}}$	
			ϕ			1	$-\frac{1}{3}$		$\frac{1}{3\sqrt{2}}$	
K^{*+}	ϕ	η	ω	K^+					0	0.17
			ϕ		$-\frac{2}{\sqrt{3}}$	$-\frac{2}{\sqrt{3}}$	$-\frac{1}{3}$	1	$-\frac{2\sqrt{2}}{9}$	
		η'	ω						0	2.6×10^{-2}
			ϕ		$\frac{1}{\sqrt{6}}$	$2\sqrt{\frac{2}{3}}$	$-\frac{1}{3}$	1	$-\frac{\sqrt{2}}{9}$	

C. The decay of the $a_2^+(1320) \to \pi^+\gamma$

This case is identical to the former ones, only the couplings change in this case. Hence we use the same formula as in the former sections and the values of the coefficients for the different diagrams of Fig. 3 are shown in Tables IX and X in the Appendix. For the momentum value in the final state $|\vec{k}|$, we use the one calculated from the physical mass of $m_{a_2} = 1320$ MeV rather than the calculated one, $m_{a_2} = 1567$ MeV. In this way we discuss essentially the coupling of the dynamically generated a_2 to $\pi\gamma$.

III. RESULTS

We evaluate the results for the two reactions where there are data, the $K_2^{*+} \to K^+\gamma$ and the $K_2^{*0} \to K^0\gamma$ decays. We include the four types of diagrams of Fig. 2, where there is exchange of pseudoscalar or vector mesons, with or without strangeness, taking into account the three channels to which the resonance couples, ρK^*, ωK^* and ϕK^*. For the case of the $a_2(1320) \to \pi^+\gamma$ we include the diagrams of Fig. 3. All the possibilities from Fig. 1 and partial widths for each different loop are given in Tables III, IV, V, VI,

TABLE V. K^{*0} decay diagrams involving the ρK^* channel and the PPV vertex.

V_1	V_2	P_l	V_f	P_f	A	B	λ	g_I	F_I	Γ_i(KeV)
K^{*0}	ρ^0	π^0	ω	K^0	$\frac{1}{\sqrt{2}}$	$\sqrt{2}$	$\frac{1}{3\sqrt{2}}$	$\frac{1}{\sqrt{3}}$	$\frac{1}{6\sqrt{3}}$	6.05
K^{*+}	ρ^-	π^+	ω	K^0	-1	$\sqrt{2}$	$\frac{1}{3\sqrt{2}}$	$-\sqrt{\frac{2}{3}}$	$\frac{1}{3\sqrt{3}}$	
ρ^-	K^{*+}	K^-	ρ^0	K^0	1	$\frac{1}{\sqrt{2}}$	$\frac{1}{\sqrt{2}}$	$-\sqrt{\frac{2}{3}}$	$-\frac{1}{2\sqrt{3}}$	0
			ω			$\frac{1}{\sqrt{2}}$	$\frac{1}{3\sqrt{2}}$		$-\frac{1}{6\sqrt{3}}$	
			ϕ			1	$-\frac{1}{3}$		$\frac{1}{3\sqrt{3}}$	
ρ^0	K^{*0}	$\bar{K}^0$	ρ^0	K^0	$-\frac{1}{\sqrt{2}}$	$-\frac{1}{\sqrt{2}}$	$\frac{1}{\sqrt{2}}$	$\frac{1}{\sqrt{3}}$	$\frac{1}{4\sqrt{3}}$	
			ω			$\frac{1}{\sqrt{2}}$	$\frac{1}{3\sqrt{2}}$		$-\frac{1}{12\sqrt{3}}$	
			ϕ			1	$-\frac{1}{3}$		$\frac{1}{6\sqrt{3}}$	
K^{*0}	ρ^0	η	ρ^0	K^0	$-\frac{2}{\sqrt{3}}$	$\frac{2}{\sqrt{3}}$	$\frac{1}{\sqrt{2}}$	$\frac{1}{\sqrt{3}}$	$-\frac{2}{3\sqrt{3}}$	6.78
		η'			$\frac{1}{\sqrt{6}}$	$\sqrt{\frac{2}{3}}$	$\frac{1}{\sqrt{2}}$	$\frac{1}{\sqrt{3}}$	$\frac{1}{6\sqrt{3}}$	0.24

TABLE VI. K^{*0} decay diagrams involving the ωK^* and ϕK^* channels and the PPV vertex.

V_1	V_2	P_l	V_f	P_f	A	B	λ	g_I	F_I	Γ_i(KeV)
K^{*0}	ω	π^0	ρ^0	K^0	$\frac{1}{\sqrt{2}}$	$\sqrt{2}$	$\frac{1}{\sqrt{2}}$	1	$\frac{1}{2}$	0.77
ω	K^{*0}	$\bar{K}^0$	ρ^0	K^0	$\frac{1}{\sqrt{2}}$	$-\frac{1}{\sqrt{2}}$	$\frac{1}{\sqrt{2}}$	1	$-\frac{1}{4}$	0.28
			ω			$\frac{1}{\sqrt{2}}$	$\frac{1}{3\sqrt{2}}$		$\frac{1}{12}$	
			ϕ			1	$-\frac{1}{3}$		$-\frac{1}{6}$	
K^{*0}	ω	η	ω	K^0	$-\frac{2}{\sqrt{3}}$	$\frac{2}{\sqrt{3}}$	$\frac{1}{3\sqrt{2}}$	1	$-\frac{2}{9}$	9.5×10^{-2}
			ϕ						0	
		η'	ω		$\frac{1}{\sqrt{6}}$	$\sqrt{\frac{2}{3}}$	$\frac{1}{3\sqrt{2}}$	1	$\frac{1}{18}$	3.4×10^{-3}
			ϕ						0	
ϕ	K^{*0}	$\bar{K}^0$	ρ^0	K^0	-1	$-\frac{1}{\sqrt{2}}$	$\frac{1}{\sqrt{2}}$	1	$\frac{1}{2\sqrt{2}}$	0.34
			ω			$\frac{1}{\sqrt{2}}$	$\frac{1}{3\sqrt{2}}$		$-\frac{1}{6\sqrt{2}}$	
			ϕ			1	$-\frac{1}{3}$		$\frac{1}{3\sqrt{2}}$	
K^{*0}	ϕ	η	ω	K^0					0	0.17
			ϕ		$-\frac{2}{\sqrt{3}}$	$-\frac{2}{\sqrt{3}}$	$-\frac{1}{3}$	1	$-\frac{2\sqrt{2}}{9}$	
		η'	ω						0	2.6×10^{-2}
			ϕ		$\frac{1}{\sqrt{6}}$	$2\sqrt{\frac{2}{3}}$	$-\frac{1}{3}$	1	$-\frac{\sqrt{2}}{9}$	

VII, VIII, IX, and X in the Appendix. The total sum of all the contributions of these diagrams is mostly constructive for the $K_2^{*+}(1430)$. In contrast, the interference between these diagrams is very destructive in the case of the $K_2^{*0}(1430)$. We have evaluated the uncertainties in the theoretical decay widths by assuming errors in the coupling constants Δg which were found to be of order 15% in Ref. [18]. The errors in Γ are obtained generating random numbers of the couplings g_i weighted by the normal (Gaussian) distribution:

$$f(x) = \frac{1}{\sigma\sqrt{2\pi}} e^{((x-g)^2/2\sigma^2)}, \tag{52}$$

for which the von Newmann rejection method is used. The average value of a sample of 30 results and its standard deviation are taken for Γ and its uncertainty. The results that we get are discussed below.

In the first place we evaluate separately the contribution of the diagram with two vectors [Fig. 1(a)] and three

TABLE VII. K^{*+} decay diagrams involving the $3V$ vertex. Terms which involve a $\gamma K^* K^*$ coupling with a neutral K^* are zero and are omitted from the table.

V_1	V_2	V_f	V_l	P_f	D	B	λ	g_I	F'_I	Γ_i (KeV)
K^{*0}	ρ^+	ρ^0	ρ^-	K^+	$\sqrt{2}$	1	$\frac{1}{\sqrt{2}}$	$-\sqrt{\frac{2}{3}}$	$\frac{1}{\sqrt{3}}$	12.8
ρ^0	K^{*+}	ρ^0	K^{*-}	K^+	$\frac{1}{\sqrt{2}}$	$\frac{1}{\sqrt{2}}$	$\frac{1}{\sqrt{2}}$	$-\frac{1}{\sqrt{3}}$	$\frac{1}{4\sqrt{3}}$	2.31
		ω			$\frac{1}{\sqrt{2}}$		$\frac{1}{3\sqrt{2}}$		$\frac{1}{12\sqrt{3}}$	
		ϕ			-1		$-\frac{1}{3}$		$\frac{1}{6\sqrt{3}}$	
ω	K^{*+}	ρ^0	K^{*-}	K^+	$\frac{1}{\sqrt{2}}$	$\frac{1}{\sqrt{2}}$	$\frac{1}{\sqrt{2}}$	1	$-\frac{1}{4}$	0.29
		ω			$\frac{1}{\sqrt{2}}$		$\frac{1}{3\sqrt{2}}$		$-\frac{1}{12}$	
		ϕ			-1		$-\frac{1}{3}$		$-\frac{1}{6}$	
ϕ	K^{*+}	ρ^0	K^{*-}	K^+	$\frac{1}{\sqrt{2}}$	1	$\frac{1}{\sqrt{2}}$	1	$-\frac{1}{2\sqrt{2}}$	0.56
		ω			$\frac{1}{\sqrt{2}}$		$\frac{1}{3\sqrt{2}}$		$-\frac{1}{6\sqrt{2}}$	
		ϕ			-1		$-\frac{1}{3}$		$-\frac{1}{3\sqrt{2}}$	

TABLE VIII. K^{*0} decay diagrams involving the $3V$ vertex. Terms which involve a $\gamma K^* K^*$ coupling with a neutral K^* are zero and are omitted from the table.

V_1	V_2	V_f	V_l	P_f	D	B	λ	g_I	F'_I	Γ_i(KeV)
K^{*+}	ρ^-	ρ^0	ρ^+	K^0	$-\sqrt{2}$	1	$\frac{1}{\sqrt{2}}$	$-\sqrt{\frac{2}{3}}$	$-\frac{1}{\sqrt{3}}$	12.8
ρ^-	K^{*+}	ρ^0	K^{*-}	K^0	$\frac{1}{\sqrt{2}}$	1	$\frac{1}{\sqrt{2}}$	$-\sqrt{\frac{2}{3}}$	$\frac{1}{2\sqrt{3}}$	9.27
		ω			$\frac{1}{\sqrt{2}}$		$\frac{1}{3\sqrt{2}}$		$\frac{1}{6\sqrt{3}}$	
		ϕ			-1		$-\frac{1}{3}$		$\frac{1}{3\sqrt{3}}$	

TABLE IX. a^+ decay diagrams involving the PPV vertex.

V_1	V_2	P_l	V_f	P_f	A	B	λ	g_I	F_I	Γ_i(KeV)
$\bar{K}^{*0}$	K^{*+}	K^+	ρ^0	π^+	-1	$\frac{1}{\sqrt{2}}$	$\frac{1}{\sqrt{2}}$	1	$-\frac{1}{2\sqrt{2}}$	1.55
			ω			$\frac{1}{\sqrt{2}}$	$\frac{1}{3\sqrt{2}}$		$-\frac{1}{6\sqrt{2}}$	
			ϕ			1	$-\frac{1}{3}$		$\frac{1}{3\sqrt{2}}$	
K^{*+}	$\bar{K}^{*0}$	K^0	ρ^0	π^+	1	$-\frac{1}{\sqrt{2}}$	$\frac{1}{\sqrt{2}}$	1	$-\frac{1}{2\sqrt{2}}$	6.2
			ω			$\frac{1}{\sqrt{2}}$	$\frac{1}{3\sqrt{2}}$		$\frac{1}{6\sqrt{2}}$	
			ϕ			1	$-\frac{1}{3}$		$-\frac{1}{3\sqrt{2}}$	
ρ^+	ω	π^0	ρ^0	π^+	$-\sqrt{2}$	$\sqrt{2}$	$\frac{1}{\sqrt{2}}$	-1	1	18.8

TABLE X. a^+ decay diagrams involving the $3V$ vertex. Terms which involve a $\gamma K^* K^*$ coupling with a neutral K^* are zero and are omitted from the table.

V_1	V_2	V_f	V_l	P_f	D	B	λ	g_I	F'_I	Γ_i(KeV)
$\bar{K}^{*0}$	K^{*+}	ρ^0	K^{*+}	π^+	$\frac{1}{\sqrt{2}}$	1	$\frac{1}{\sqrt{2}}$	1	$-\frac{1}{2\sqrt{2}}$	8.9
		ω			$\frac{1}{\sqrt{2}}$		$\frac{1}{3\sqrt{2}}$		$-\frac{1}{6\sqrt{2}}$	
		ϕ			-1		$-\frac{1}{3}$		$-\frac{1}{3\sqrt{2}}$	
ω	ρ^+	ρ^0	ρ^+	π^+	$\sqrt{2}$	$\sqrt{2}$	$\frac{1}{\sqrt{2}}$	-1	1	8.6

vectors [Fig. 1(b)]. The results (without error estimated) obtained are

$$\begin{aligned}
\Gamma_{(K_2^{*+}(1430)\to K^+\gamma),PPV} &= 46.6\ \text{KeV},\\
\Gamma_{(K_2^{*+}(1430)\to K^+\gamma),3V} &= 28.2\ \text{KeV},\\
\Gamma_{(K_2^{*0}(1430)\to K^0\gamma),PPV} &= 0.19\ \text{KeV},\\
\Gamma_{(K_2^{*0}(1430)\to K^0\gamma),3V} &= 0.29\ \text{KeV},\\
\Gamma_{(a^+(1320)\to \pi^+\gamma),PPV} &= 65.7\ \text{KeV},\\
\Gamma_{(a^+(1320)\to \pi^+\gamma),3V} &= 34.8\ \text{KeV}.
\end{aligned} \tag{53}$$

This is done only for the purpose of showing that the contributions of the two mechanisms are of the same order of magnitude, which means that both are important and must be taken into account.

In order to obtain the decay width one must sum the amplitudes of the two mechanisms, which are constructive in the cases of the K_2^{*+} and a_2^+, and destructive in the case of the K_2^{*0}. We have seen that in the case of the K_2^{*0} we obtain a complete cancellation of the amplitudes when the masses of the pseudoscalar mesons are made equal and also those of the nonet of vectors. Thus, the result seems to be tied to the neutral charge of the K_2^{*0}, providing the same result as quark models for the same reason. The small finite results that we obtain are due to the use of the physical masses within the SU(3) multiplets.

The final results obtained from the sum of the amplitudes of both types, including uncertainties evaluated according to the discussion around Eq. (52), are the following

$$\begin{aligned}
\Gamma(K_2^{*+}\to K^+\gamma) &= 150 \pm 50\ \text{KeV}\\
\Gamma(K_2^{*0}\to K^0\gamma) &= (1.0\pm 0.8)\times 10^{-2}\ \text{KeV}
\end{aligned} \tag{54}$$

$$\Gamma(a_2(1320)\to \pi^+\gamma) = (196\pm 30)\ \text{KeV}. \tag{55}$$

These results should be compared with the experimental widths

$$\begin{aligned}
\Gamma(K_2^{*+}\to K^+\gamma) &= 236 \pm 50\ \text{KeV}\\
\Gamma(K_2^{*0}\to K^0\gamma) &= <98\ \text{KeV}\\
\Gamma(a_2^+(1320)\to \pi^+\gamma) &= 281\pm 34\ \text{KeV}
\end{aligned} \tag{56}$$

where we have summed in quadrature the error in the branching ratio of Eq. (1) and the one of the total width of the PDG. As we can see, the result for the charged K_2^{*+} is compatible with the data within errors and for the one of the neutral K_2^{*0} we can see that the width for $K_2^{*0}\to K^0\gamma$ is very small compared to the $K_2^{*+}\to K^+\gamma$ and the upper bound is fulfilled. It would be interesting to have this upper bound improved experimentally, since we predict such a small number for the width.

For the case of the $a_2(1320)$ the agreement with data can be considered qualitatively. Considering errors the maximum theoretical value would be 226 KeV and the minimum experimental one 247 KeV. Let us mention that we have not changed the values of the coupling constants of [18]. Should one redo the evaluation of these couplings with an improved mass for this resonance we should expect small variations, adding to our present error estimates. Yet, the large mass difference between the state obtained in [18] and the experimental one should be taken as an indication that further components to VV should be present in the physical state $a_2(1320)$, so there is no point in demanding a more accurate agreement with data. In any case it is more indicative to see the ratio of $\Gamma(K_2^{*+}\to K^+\gamma)/\Gamma(a_2^+\to\pi^+\gamma)$ which in our case is 0.77 ± 0.30 compared to the experiment 0.84 ± 0.20, which show a good overlap.

IV. CONCLUSIONS

We have studied the decay of the $K_2^{*+}(1430)$, $K_2^{*0}(1430)$ and $a_2(1320)$ into a photon and a pseudoscalar meson. The states considered are those generated dynamically from the vector-vector interaction in [18] that can be assigned to known resonances and that decay in this mode. The evaluation of the width required the consideration of loop diagrams involving the coupling of the resonances to the constituent vector-vector channels, plus some anomalous couplings. We find that the loops become convergent and we can evaluate finite values for the decay rates by making an approximation consistent with the VV molecular picture. The results obtained for the width of the $K_2^{*+}(1430)$ are well within the experimental values considering errors. For the case of the $K_2^{*0}(1430)$ we found a very small width, well below the experimental upper bound of the PDG. It would be worth trying to improve on this boundary since our results are so much smaller than the present bound. The case of the $a_2(1320)$ is a bit more problematic, since the mass obtained theoretically is 1560 MeV with standard values of the subtraction constants. Yet, we found qualitative agreement between the results of the $a_2^+\to\pi^+\gamma$ with the experiment for $a_2^+(1320)\to\pi^+\gamma$. The agreement with experiment is better for the ratio of $\Gamma(K_2^{*+}\to K^+\gamma)/\Gamma(a_2^+\to\pi^+\gamma)$.

In any case it is worth stating that our picture for these states as molecular states of vector-vector is passing repeatedly the different test demanded by experiment, as the one presented here and those commented in the Introduction. The results obtained are adding progressive support to the idea of the $K_2^*(1430)$ and other related resonances found in [18] as dynamically generated from the vector-vector interaction.

Nevertheless, in spite of all the arguments given in favor of the dynamically generated vector-vector states, the fact remains that the tensor states $f_2(1270)$, $f_2'(1525)$, $a_2(1320)$, $K_2^*(1430)$ are well reproduced in the quark model, including many of their decay modes (see, e.g., [23–29]). This success in both models may reflect the fact that the constituent quarks in quark models are objects effectively dressed with meson clouds and the overlap between the molecular picture and the quark model picture could be bigger than expected in some cases [47]. It remains to see if future measurements of new magnitudes could prove that one picture is more adequate than the other to represent an, admittedly, more complex nature. For the moment we have shown that the molecular picture has passed this nontrivial test, often suggested as crucial to learn about the nature of hadronic states.

ACKNOWLEDGMENTS

This work is partly supported by DGICYT Contract No. FIS2006-03438. We acknowledge the support of the European Community-Research Infrastructure Integrating Activity Study of Strongly Interacting Matter (acronym HadronPhysics2, Grant Agreement No. 227431) under the Seventh Framework Programme of EU. A. H. is supported in part by the Grant for Scientific Research Contract No. 19540297 from the Ministry of Education, Culture, Science and Technology, Japan. H. N. is supported by the Grant for Scientific Research No. 18-8661 from JSPS

[1] M. R. Pennington, Nucl. Phys. B, Proc. Suppl. **181-182**, 251 (2008).
[2] C. Amsler, Phys. Lett. B **541**, 22 (2002).
[3] M. Doring, Nucl. Phys. **A786**, 164 (2007).
[4] T. Branz, T. Gutsche, and V. E. Lyubovitskij, Phys. Rev. D **78**, 114004 (2008).
[5] Y. Dong, A. Faessler, T. Gutsche, S. Kovalenko, and V. E. Lyubovitskij, Phys. Rev. D **79**, 094013 (2009).
[6] T. Branz, T. Gutsche, and V. E. Lyubovitskij, Phys. Rev. D **82**, 054025 (2010).
[7] Y. Dong, A. Faessler, T. Gutsche, S. Kumano, and V. E. Lyubovitskij, Phys. Rev. D **82**, 034035 (2010).
[8] T. Branz, T. Gutsche, and V. E. Lyubovitskij, Phys. Rev. D **82**, 054010 (2010).
[9] X. Liu and H. W. Ke, Phys. Rev. D **80**, 034009 (2009).
[10] J. A. Oller, E. Oset, and A. Ramos, Prog. Part. Nucl. Phys. **45**, 157 (2000).
[11] E. Oset, D. Cabrera, V. K. Magas, L. Roca, S. Sarkar, M. J. Vicente Vacas, and A. Ramos, Pramana **66**, 731 (2006).
[12] J. A. Oller and E. Oset, Nucl. Phys. **A620**, 438 (1997); **652**, 407 (1999).
[13] N. Kaiser, Eur. Phys. J. A **3**, 307 (1998).
[14] J. A. Oller, E. Oset, and J. R. Pelaez, Phys. Rev. Lett. **80**, 3452 (1998).
[15] J. A. Oller, E. Oset, and J. R. Pelaez, Phys. Rev. D **59**, 074001 (1999); **60**, 099906(E) (1999); **75**, 099903(E) (2007).
[16] V. E. Markushin, Eur. Phys. J. A **8**, 389 (2000).
[17] R. Molina, D. Nicmorus, and E. Oset, Phys. Rev. D **78**, 114018 (2008).
[18] L. S. Geng and E. Oset, Phys. Rev. D **79**, 074009 (2009).
[19] R. Molina, H. Nagahiro, A. Hosaka, and E. Oset, Phys. Rev. D **80**, 014025 (2009).
[20] R. Molina and E. Oset, Phys. Rev. D **80**, 114013 (2009).
[21] R. Molina, T. Branz, and E. Oset, Phys. Rev. D **82**, 014010 (2010).
[22] C. Amsler *et al.* (Particle Data Group), Phys. Lett. B **667**, 1 (2008).
[23] D. M. Li, H. Yu, and Q. X. Shen, J. Phys. G **27**, 807 (2001).
[24] E. Klempt and A. Zaitsev, Phys. Rep. **454**, 1 (2007).
[25] V. Crede and C. A. Meyer, Prog. Part. Nucl. Phys. **63**, 74 (2009).
[26] S. Godfrey and N. Isgur, Phys. Rev. D **32**, 189 (1985).
[27] T. Barnes, F. E. Close, P. R. Page, and E. S. Swanson, Phys. Rev. D **55**, 4157 (1997).
[28] T. Barnes, N. Black, and P. R. Page, Phys. Rev. D **68**, 054014 (2003).
[29] A. V. Anisovich, V. V. Anisovich, M. A. Matveev, and V. A. Nikonov, Yad. Fiz. **66**, 946 (2003) [Phys. At. Nucl. **66**, 914 (2003)].
[30] H. Nagahiro, J. Yamagata-Sekihara, E. Oset, S. Hirenzaki, and R. Molina, Phys. Rev. D **79**, 114023 (2009).
[31] T. Branz, L. S. Geng, and E. Oset, Phys. Rev. D **81**, 054037 (2010).
[32] A. Martinez Torres, L. S. Geng, L. R. Dai, B. X. Sun, E. Oset, and B. S. Zou, Phys. Lett. B **680**, 310 (2009).
[33] L. S. Geng, F. K. Guo, C. Hanhart, R. Molina, E. Oset, and B. S. Zou, Eur. Phys. J. A **44**, 305 (2010).
[34] M. Bando, T. Kugo, S. Uehara, K. Yamawaki, and T. Yanagida, Phys. Rev. Lett. **54**, 1215 (1985).
[35] M. Bando, T. Kugo, and K. Yamawaki, Phys. Rep. **164**, 217 (1988).
[36] M. Harada and K. Yamawaki, Phys. Rep. **381**, 1 (2003).
[37] U. G. Meissner, Phys. Rep. **161**, 213 (1988).
[38] H. Nagahiro, L. Roca, A. Hosaka, and E. Oset, Phys. Rev. D **79**, 014015 (2009).
[39] D. Gamermann, E. Oset, and B. S. Zou, Eur. Phys. J. A **41**, 85 (2009).
[40] G. Ecker, J. Gasser, H. Leutwyler, A. Pich, and E. de Rafael, Phys. Lett. B **223**, 425 (1989).
[41] U. G. Meissner, Phys. Rep. **161**, 213 (1988).
[42] E. Pallante and R. Petronzio, Nucl. Phys. **B396**, 205 (1993).
[43] H. Nagahiro, L. Roca, and E. Oset, Eur. Phys. J. A **36**, 73 (2008).
[44] T. Branz, T. Gutsche, and V. E. Lyubovitskij, Phys. Rev. D **78**, 114004 (2008).
[45] A. Bramon, A. Grau, and G. Pancheri, Phys. Lett. B **283**, 416 (1992).
[46] E. Oset, J. R. Pelaez, and L. Roca, Phys. Rev. D **67**, 073013 (2003).
[47] P. Gonzalez (private communication).